On-Chip Electric Field Driven Electrochemical Detection Using a Poly(dimethylsiloxane) Microchannel with Gold Microband Electrodes

ARTICLE *in* ANALYTICAL CHEMISTRY · JUNE 2008

Impact Factor: 5.64 · DOI: 10.1021/ac702570p · Source: PubMed

6 AUTHORS, INCLUDING:

Francisco Javier del Campo
Spanish National Research Council
124 PUBLICATIONS **2,150** CITATIONS

SEE PROFILE

Francesc Xavier Muñoz Pascual
Barcelona Microelectronics Institute
101 PUBLICATIONS **1,861** CITATIONS

SEE PROFILE

Leif Nyholm
Uppsala University
163 PUBLICATIONS **3,631** CITATIONS

SEE PROFILE

Anal. Chem. **2008,** *80,* 3622–3632

On-Chip Electric Field Driven Electrochemical Detection Using a Poly(dimethylsiloxane) Microchannel with Gold Microband Electrodes

Olga Ordeig,[†,‡] Neus Godino,[†] Javier del Campo,[†] Francesc Xavier Muñoz,[†] Fredrik Nikolajeff,[§] and Leif Nyholm*,[||]

Centro Nacional de Microelectrónica, IMB-CNM, CSIC, Campus de la Universidad, Autónoma de Barcelona, Esfera UAB, Bellaterra-08193, Spain, Department of Engineering Sciences, The Ångström Laboratory, Uppsala University, Box 534, SE-751 21 Uppsala, Sweden, and Department of Materials Chemistry, The Ångström Laboratory, Uppsala University, Box 538, SE-751 21 Uppsala, Sweden

An external electric field driven in-channel detection technique for on-chip electrochemical detection in micro fabricated devices is described based on a microfluidic system containing an array of 20 microband electrodes. It is shown that an external electric field induces a potential difference between two gold microband electrodes in a poly(dimethylsiloxane) (PDMS) microchannel, and that this enables the electrochemical detection of electroactive species such as ascorbic acid and $Fe(CN)_6^{4-}$. The results, which are supported by simulations of the behavior of the microband electrodes in the microfluidic system, show that the induced potential difference between the electrodes can be controlled by altering the external electric field or by using different microbands in the microband array. As the obtained currents depend on the concentrations of electroactive species in the flowing solution and the detection can be carried out anywhere within the channel without interference of the external electric field, the present approach significantly facilitates electrochemical detection in capillary electrophoresis. This approach consequently holds great promise for application in inexpensive portable chip-based capillary electrophoresis (CE) devices.

Microfluidics provides a way to miniaturize chemical analysis systems and can therefore enable rapid, low cost analyses that generate little chemical waste. Much effort has therefore been made to develop analytical devices based on microfluidic systems. Miniaturized electrophoresis devices have, up to now and by far, been the most widely developed devices due to their scalability and compatibility with the substrates available for device construction.[1,2] Electrophoresis has been used on-chip not only as a separation technique but also for fluid transport and mixing. A significant advantage of using electrokinetically driven flow is that valves and macroscopic pumps become redundant when injecting and moving liquid samples.[3] Although capillary electrophoresis (CE) is frequently used in conjunction with absorbance and fluorescence detection,[4] electrochemical detection methods are receiving increasing attention for on-chip capillary electrophoresis applications due to their relatively low cost, high sensitivity, and portability.[5] Among electrochemical techniques, amperometric detection has been the most widely employed method in on-chip applications, since first described in 1987 by Wallingford and Ewing.[6] The main problems of using electrochemical detection in (conventional as well as on-chip) CE are caused by interferences due to the presence of the CE electric field[7] and uncertainties in the positioning of the electrodes with respect to the capillary, which may affect the reproducibility of the measurements.[8,9] The latter problem can, however, be minimized by the use of microfabricated systems in which the positions of the electrodes are fixed during the microfabrication process.[10–14] Reviews on the microfabrication of devices and/or applications involving electrochemical detection in on-chip capillary electrophoresis have also been published.[8,9,15,16]

* Corresponding author. E-mail: Leif.Nyholm@mkem.uu.se. Phone: +46 18 4713742.

† Campus de la Universidad, Autónoma de Barcelona.

‡ Present address: MIC-Department of Micro and Nanotechnology, DTU-Building 345east, DK-2800 Kongens Lyngby, Denmark.

§ Department of Engineering Sciences, The Ångström Laboratory, Uppsala University.

|| Department of Materials Chemistry, The Ångström Laboratory, Uppsala University.

(1) Effenhauser, C. S.; Bruin, G. J. M.; Paulus, A. *Electrophoresis* **1997**, *18*, 2203–2213.
(2) Lacher, N. A.; Garrison, K. E.; Martin, R. S.; Lunte, S. M. *Electrophoresis* **2001**, *22*, 2526–2536.
(3) Stone, H. A.; Stroock, A. D.; Ajdari, A. *Annu. Rev. Fluid Mech.* **2004**, *36*, 381–411.
(4) Dolnik, V.; Liu, S. R.; Jovanovich, S. *Electrophoresis* **2000**, *21*, 41–54.
(5) Wang, J. *Talanta* **2002**, *56*, 223–231.
(6) Wallingford, R. A.; Ewing, A. G. *Anal. Chem.* **1987**, *59*, 1762–1766.
(7) Wang, K.; He, F. Y.; Liu, A. L.; Xu, J. J.; Chen, H. Y.; Xia, X. H. *Langmuir* **2006**, *22*, 7052–7058.
(8) Nyholm, L. *Analyst* **2005**, *130*, 599–605.
(9) Xu, J.-J.; Wang, A.-J.; Chen, H.-Y. *Trends Anal. Chem.* **2007**, *26*, 125–132.
(10) Dossi, N.; Toniolo, R.; Pizzariello, A.; Susmel, S.; Perennes, F.; Bontempelli, G. *J. Electroanal. Chem.* **2007**, *601*, 1–7.
(11) Yao, X.; Wang, J.; Zhang, L. Y.; Yang, P. Y.; Chen, G. *Talanta* **2006**, *69*, 1285–1291.
(12) Tsai, D.-M.; Lin, K.-W.; Zen, J.-M.; Chen, H.-Y.; Hong, R.-H. *Electrophoresis* **2005**, *26*, 3007–3012.
(13) Tsai, D.-M.; Tai, K.-W.; Shih, P.-R.; Chang, R.-L.; Wu, H.; Conte, E.-D.; Zen, J.-M. *Electroanalysis* **2005**, *17*, 1991–1994.
(14) Castano-Alvarez, M.; Fernandez-Abedul, M. T.; Costa-Garcia, A. *J. Chromatogr., A* **2006**, *1109*, 291–299.
(15) Pumera, M.; Merkoci, A.; Alegret, S. *Trends Anal. Chem.* **2006**, *25*, 219–235.

10.1021/ac702570p CCC: $40.75
Published on Web 04/03/2008

In general, the influence of the CE high voltage on electrochemical measurements results in high levels of noise and shifts in the detection potentials. To avoid or minimize these effects, either decouplers[17–20] or end-column detection[13,21–24] is currently used. In the first case, a new pathway for the CE current to ground is generated while the second approach is based on the fact that the potential drop at the end of narrow capillaries is small enough to allow amperometric detection. Although the end-column detection approach generally is the preferred decoupling method in conjunction with on-chip devices due to its less complicated implementation,[8] the use of palladium based decouplers has also been described.[19,20]

With the end-column detection approach, several techniques have been described to reduce the magnitude of the shift in the detection potential introduced by the separation electric field. One approach is based on the fact that the shift is decreased if the conductivity of the solution immediately outside the separation channel is increased.[8] Another possibility is to increase the distance between the working electrode and the end of the channel.[8,25,26] This, however, gives rise to increased band broadening. To enable electrochemical detection in the presence of the separation electric field, a floating high-voltage separation power supply[27] or an isolated potentiostat[10,28] can be employed. It should, however, be pointed out that this does not eliminate the shift in the potential between the working and the reference electrode induced by the separation electric field. Klett et al.[29] have, on the other hand, shown that the shift can be eliminated if the working and reference electrode are positioned in such a way that both electrodes are exposed to the same separation electric field induced potential. It was also shown[29] that the shift in the working electrode potential can be determined merely by measuring the potential difference between the working and reference electrode in the presence and absence of the separation electric field. A similar technique was employed by Forry et al.,[30] who used the shift in cyclic voltammetry peak potentials to determine the potential needed to compensate for the influence of the electric field when employing electrochemical detection in an electrophoresis channel.

While many reports have been devoted to the elimination of the influence of the CE separation electric field on electrochemical detection, a few groups have instead made use of the separation electric field in novel detection techniques.[31–34] Manz and coworkers[31] thus described a wireless electrochemiluminescence detector based on potential differences induced by a CE separation electric field while Klett and Nyholm[33] described a potentiostatless amperometric detection technique based on the use of the potential induced between microband electrodes positioned at different locations within the separation electric field. A technique analogous to the latter approach was subsequently used by Xu et al.[34] to determine electroinactive species based on the amperometric response of the oxygen dissolved in the solution. The presence of the CE separation electric field can also be used for conductivity detection as was demonstrated by Girault and coworkers.[32] A significant advantage of the separation electric field driven detection techniques is that this type of detection can be carried out anywhere within the separation channel. In the amperometric mode, which generally constitutes a very sensitive electrochemical detection technique, it would also be possible to alter the detection potential merely by selecting different pairs of electrodes with different locations within the channel. The use of many pairs of electrodes should also allow simultaneous detection at a number of different potentials. As Klett and Nyholm[33] merely used microband electrodes positioned at the end of a fused silica capillary to demonstrate electric field driven amperometric detection, further studies are, however, required to investigate the possibilities of the latter approach for on-chip detection within a microfabricated channel.

In this article, we describe an example of on-chip separation electric field driven amperometric detection. It is based on the use of a microfabricated flow system containing an array of 20 gold microband electrodes. The microband electrodes were characterized using cyclic voltammetry at different flow rates, and the obtained results were compared with simulations based on a two-dimensional model. In the presence of an external electric field, the potential difference between two microbands is shown to depend on the distance between the microbands and the electric field strength. The presence of this potential difference enables in-channel amperometric detection to be carried out in the absence of a potentiostat as is demonstrated for the oxidation of ascorbic acid and $Fe(CN)_6^{4-}$.

EXPERIMENTAL SECTION

Chemicals. Potassium hexacyanoferrate(II) (K_4FeCN_6), potassium hexacyanoferrate(III) (K_3FeCN_6), and ascorbic acid were supplied by Merck. Potassium nitrate was purchased from VWR (Prolabo). Sulfuric acid and 2-propanol (>99%) were obtained from Sigma-Aldrich. All chemicals were of analytical reagent grade, and all aqueous solutions were prepared using ultrapure deionized water (DI) (18 MΩ cm).

The microchannel substrates were produced by casting a mixture of poly(dimethyl siloxane) (PDMS) monomer and curing agent from Wacker-Chemie GmbH (München, Germany) on resist

(16) Wang, J. *Electroanalysis* **2005**, *17*, 1133–1140.
(17) Vickers, J. A.; Henry, C. S. *Electrophoresis* **2005**, *26*, 4641–4647.
(18) Kim, J. H.; Kang, C. J.; Jeon, D.; Kim, Y. S. *Microelectron. Eng.* **2005**, *78–79*, 563–570.
(19) Dawoud, A. A.; Kawaguchi, T.; Jankowiak, R. *Anal. Bioanal. Chem.* **2007**, *388*, 245–252.
(20) Mecker, L. C.; Martin, R. S. *Electrophoresis* **2006**, *27*, 5032–5042.
(21) Woods, L. A.; Ewing, A. G. *ChemPhysChem* **2003**, *4*, 207–211.
(22) Wang, J.; Chen, G.; Chatrathi, M. P.; Fujishima, A.; Tryk, D. A.; Shin, D. *Anal. Chem.* **2003**, *75*, 935–939.
(23) Wang, J.; Pumera, M.; Chatrathia, M. P.; Rodriguez, A.; Spillman, S.; Martin, R. S.; Lunte, S. M. *Electroanalysis* **2002**, *14*, 1251–1255.
(24) Wang, J.; Chen, G.; Chatrathi, M. P.; Musameh, M. *Anal. Chem.* **2004**, *76*, 298–302.
(25) Wallenborg, S. R.; Nyholm, L.; Lunte, C. E. *Anal. Chem.* **1999**, *71*, 544–549.
(26) Matysik, F.-M. *J. Chromatogr., A* **1996**, *742*, 229–234.
(27) Hebert, N. E.; Kuhr, W. G.; Brazill, S. A. *Anal. Chem.* **2003**, *75*, 3301–3307.
(28) Martin, R. S.; Ratzlaff, K. L.; Huynh, B. H.; Lunte, S. M. *Anal. Chem.* **2002**, *74*, 1136–1143.
(29) Klett, O.; Björefors, F.; Nyholm, L. *Anal. Chem.* **2001**, *73*, 1909–1915.
(30) Forry, S. P.; Murray, J. R.; Heien, M.; Locascio, L. E.; Wightman, R. M. *Anal. Chem.* **2004**, *76*, 4945–4950.
(31) Arora, A.; Eijkel, J. C. T.; Morf, W. E.; Manz, A. *Anal. Chem.* **2001**, *73*, 3282–3288.
(32) Bai, X. X.; Wu, Z. Y.; Josserand, J.; Jensen, H.; Schafer, H.; Girault, H. H. *Anal. Chem.* **2004**, *76*, 3126–3131.
(33) Klett, O.; Nyholm, L. *Anal. Chem.* **2003**, *75*, 1245–1250.
(34) Xu, J. J.; Bao, N.; Xia, X. H.; Peng, Y.; Chen, H. Y. *Anal. Chem.* **2004**, *76*, 6902–6907.

structured silicon wafers. SU-8 50 resist for master structuring was purchased from MicroChem (Newton). The conductive epoxy used to provide electric contact between the chip and the electrode connectors was supplied by Circuit Works (Lake Bluff).

Instrumentation. The cyclic voltammetric experiments were carried out with an Autolab (Eco-Chemie, Utrect, The Netherlands) system interfaced to a PC using the GPES (version 4.9) software for Windows. A PHD2000 infusion syringe pump (Harvard Apparatus, Holliston) and silicon tubing with an inner diameter of 0.56 mm (from Elfa, Järfälla, Sweden) were used to obtain a flow of solution through the microfluidic channel. The volumetric flow rates used in this work ranged from 1 to 10 μL min^{-1}. In the flow electrochemical measurements, a three electrode cell configuration was used with two microbands acting as working and counter electrodes and an additional microband as a quasi-reference electrode. The counter and reference electrodes were located downstream with respect to the working electrode to avoid interferences due to the counter electrode reactions.[35] Prior to the experiments, the gold microband electrodes were electrochemically activated by cycling the potential from −0.2 to +0.8 V (vs Au quasi-reference electrode) in a solution containing 0.050 M H_2SO_4 and 0.5 M KNO_3.

In the external electric field experiments, the potential difference and current between two gold microband electrodes were recorded using a Keithley 197A voltmeter and a Keithley 485 picoamperemeter (Keithley Instruments, Cleveland), respectively. The external electric field was obtained with a dc power supply by applying a potential difference of up to 50 V between two steel needles placed inside the silicon tubing at the inlet and the outlet of the microfluidic cell. All external electric field experiments were performed under laminar flow conditions employing a flow rate of 5 μL min^{-1}.

Microfabrication Procedures. The microfluidic device was manufactured through the assembly of two separate parts, an upper PDMS part containing the microfluidic channel and reservoir elements and a lower part containing the microband gold electrodes patterned on a Pyrex substrate. Schematic top and sideviews of the devices are shown in Figure 1.

The SU-8 master utilized in the manufacturing of the microfluidic channel was fabricated on a 4 in. standard silicon wafer using soft-lithography. The first step of the fabrication process consisted of a careful cleaning of the wafer (using Standard Clean One (SC-1, $NH_4OH/H_2O_2/H_2O$, 65 °C) and Standard Clean Two (SC-2, HCl/H_2O_2, H_2O, 65 °C)) to guarantee good resist adherence. SU-8 50 resist was then spun on the wafer followed by prebaking, exposure to UV light through a CAD-designed chrome mask, and postbaking according to the supplier's recipe. The resist-coated wafer was developed and hard-baked for 30 min at 150 °C. The height and width of the resist pattern were found to be 77 and 95 μm, respectively, when measured with an optical profiler (Vecco, Woodbury). The inverse image of the SU-8 resist pattern was produced by casting PDMS polymer on the structured masters. PDMS prepolymer and curing agent were mixed (10:1 w/w). Air bubbles were removed by letting the PDMS mixture rest for an hour at –20 °C. The polymer mixture was poured over the masters and cured for 1 h at 70 °C in a furnace. After the structures were allowed to cool down, to avoid deformations, the polymer was peeled off from the masters. Reservoir cavities were then punched in the substrate containing the channels. Small dice of cured PDMS containing a hole with a diameter of 0.56 mm were then bonded over the reservoirs by corona discharge. These dice facilitated the connection of silicon tubing to the microfluidic devices.

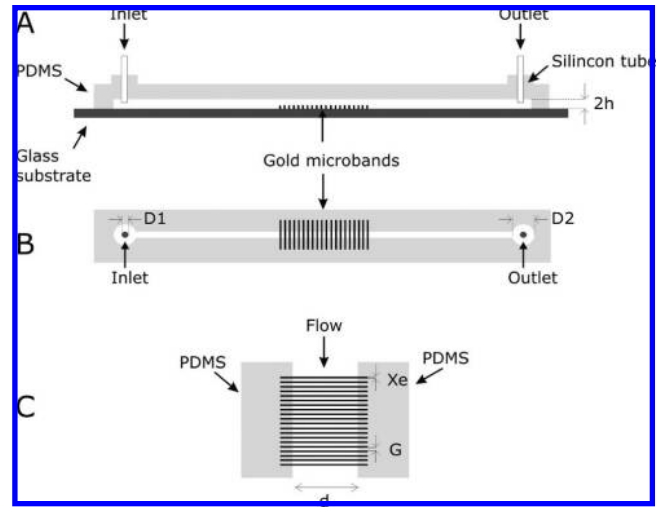

Figure 1. (A) Lateral and (B) top views of the microfluidic devices used in this work. (C) View of microband electrodes (Xe = 20 μm, G = 50 or 250 μm, d = 95 μm) in the microchannel ($2h$ = 77 μm, d = 95 μm).

The lower Pyrex part of the microfluidic containing 20 parallel gold band electrodes each with a width of 20 μm and separated from their closest neighbor by either 50 or 250 μm was manufactured by lithographic and lift-off techniques. The electrode pattern was defined by a chrome optical mask replicated by lithography into a thin S-1813 photoresist layer spin coated on the Pyrex wafer. A 20 nm adhesion layer of Ti and a 100 nm layer of Au were then evaporated over the developed resist pattern. Once the desired metals had been deposited, the underlying resist was stripped in acetone. Unwanted metallic parts were lifted off, leaving the desired electrode pattern on the wafer. The chips were individually cut from the wafer using a diamond saw.

The PDMS microchannel part and the microelectrode array part were finally bonded together. Prior to this step, the surfaces of both parts were carefully cleaned with 2-propanol and deionized water to increase their hydrophobicity. After the surfaces were dried, the PDMS piece was exposed to corona discharge for about 25 s using a Tesla coil (ETP, Chicago, IL). The PDMS part was then placed perpendicularly over the set of parallel microbands on the Pyrex substrate. The closed structure was next kept at 70 °C during 1 h to produce irreversible bonding between the Pyrex and PDMS surfaces.

As is seen in Figure 1C, the effective length of the microband electrodes in the microchannel was defined by the microchannel width. The area of each microband electrode was hence 1.9×10^{-5} cm^2. The optical transparency of the PDMS allowed microscopic examinations of the state of the band electrodes during the experiments.

Safety Considerations. To avoid electrical shocks, the power supply should be handled with care.

(35) Wang, J. *Analytical Electrochemistry*; Wiley-VCH: New York, 2001.

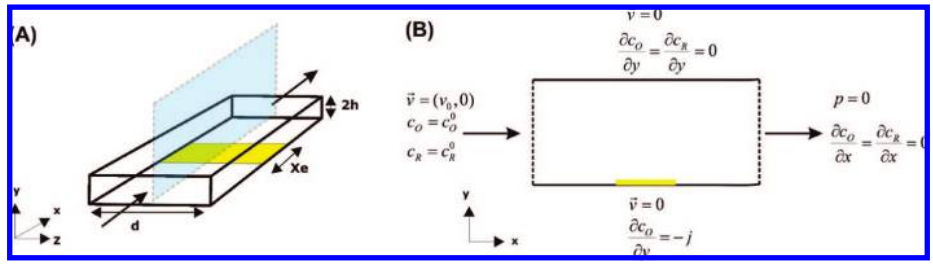

Figure 2. (A) Three-dimensional view of a band microelectrode placed inside a microchannel, where 2*h* is the height of the channel (77 μm), *d* is the electrode width (95 μm), and x_e is the length of the band electrode (20 μm). The arrows show the flow direction. (B) Perpendicular plane of the microchannel used for the two-dimensional model simulations. The boundary conditions for the mass transport and fluid movement were defined next to the correspondent surface, where the straight lines represent the walls of the microchannel and the dashed lines the inlet and outlet, respectively.

SIMULATION

In this work, we used finite element techniques to characterize the microfluidic behavior of the device. The aim is to use the current measured at the microelectrodes in the microchannel to calibrate the flow. The presence of tiny leaks is common in this kind of PDMS microfluidic devices, and they are often quite difficult to avoid. The presence of leaks leads to an overestimation of the flow during the measurements. The simulation of microelectrode voltammetric characterization let us estimate the real flow inside the cell. Several authors have used electrochemical measurements or simulations in order to determine a range of fluidic parameters. Amatore et al.[36,37] present a method to reconstruct the velocity profile of a fluid flowing through a rectangular section channel, which is based on electrochemical simulations. Thompson and Compton[38] also studied the effect of the hydrodynamic velocity profile in electrochemical currents. In this case, they focus their work on the hydrodynamic information at the inlet of the channel, where the parabolic velocity profile is not achieved.

The two-dimensional model used in the simulations of the mass transport controlled limiting currents in the microfluidic channel, depicted in Figure 1, is based on mass transport by diffusion and convection. Migration effects were neglected as an excess of supporting electrolyte was used in the experiments. In the present work, we consider a reversible one-electron reduction of species O at the microband electrode:

$$O + e^- \rightleftharpoons R \tag{1}$$

Assuming that the electrode is fast enough to ensure that the current is mass transport limited,[39] then the current is given by the Levich expression.[40] For a microband electrode inside a rectangular section channel, it can be expressed as[41]

$$I = 0.925nFcw(x_eD)^{2/3}\left(\frac{4}{3}\frac{v_{max}}{h}\right)^{1/3} \tag{2}$$

where n is the number of exchanged electrons, F is the Faraday constant, c and D are the concentration and the diffusion coefficient of the electroactive species, h is half-the-height of the channel, x_e and w are the length and the width of the microband electrode and v_{max} is the maximum linear velocity. The latter was derived neglecting the axial diffusion as only axial convection and normal diffusion are relevant in a macroscopic system. In contrast to the Levich equation,[40] our simulations consider both axial and normal diffusion.

The influence of axial diffusion can, however, be significant for microelectrodes at low flow rates. To take this effect into account, the 2D rectangular section of the channel described in the Experimental Section was modeled. Figure 2 is a schematic representation of the two-dimensional channel section used and the boundary conditions assumed in the model used for the simulations. It is important to take in consideration that the electrode should be positioned sufficiently far from the inlet so that a Poiseuille profile is completely developed.[40] In our case the maximum inlet region is around 3 μm for a 10 μL min^{-1} flow rate. Under these conditions, the steady-state mass transport equation of the reactant, O, in the cell is

$$D_O\left(\frac{\partial^2 c_O}{\partial x^2} + \frac{\partial^2 c_O}{\partial y^2}\right) - \left(v_x\frac{\partial c_O}{\partial x} + v_y\frac{\partial c_O}{\partial y}\right) = 0 \tag{3}$$

where c_O is the concentration and D_O is the diffusion coefficient of species O, and (v_x,v_y) are the components of the velocity vector in the channel. To obtain the velocity field, the fluid is considered Newtonian and incompressible, so the steady-state incompressible Navier–Stokes (eq 4) and the continuity equation (eq 5) should be solved:

$$\begin{aligned}\rho\left(v_x\frac{\partial v_x}{\partial x} + v_y\frac{\partial v_x}{\partial y}\right) - \eta\left(\frac{\partial^2 v_x}{\partial x^2} + \frac{\partial^2 v_x}{\partial y^2}\right) + \frac{\partial p}{\partial x} = 0\\ \rho\left(v_x\frac{\partial v_y}{\partial x} + v_y\frac{\partial v_y}{\partial y}\right) - \eta\left(\frac{\partial^2 v_y}{\partial x^2} + \frac{\partial^2 v_y}{\partial y^2}\right) + \frac{\partial p}{\partial y} = 0\end{aligned} \tag{4}$$

$$\frac{\partial v_x}{\partial x} + \frac{\partial v_y}{\partial y} = 0 \tag{5}$$

where ρ and η are the density and the viscosity of the fluid, respectively, and p is the pressure. The boundary condition at the electrode is that the flux through the electrode is controlled by the applied potential, E, via the Butler–Volmer equation:[39]

(36) Amatore, C.; Klymenko, O. V.; Svir, I. *ChemPhysChem* **2006**, *7*, 482–487.
(37) Amatore, C.; Oleinick, A.; Klymenko, O. V.; Svir, I. *ChemPhysChem* **2005**, *6*, 1581–1589.
(38) Thompson, M.; Compton, R. G. *Anal. Chem.* **2007**, *79*, 626–631.
(39) Bard, A. J.; Faulkner, L. R. *Electrochemical Methods: Fundamentals and Applications*; Wiley: Chichester, U.K., 2001.
(40) Levich, V. G. *Physicochemical Hydrodynamics*; Prentice Hall: Englewood Cliffs, NJ, 1962.
(41) Compton, R. G.; Fisher, A. C.; Wellington, R. G.; Dobson, P. J.; Leigh, P. A. *J. Phys. Chem.* **1993**, *97*, 10410–10415.

$$j = j_0 \frac{c_O}{c_O^0} \exp\left[\frac{-\alpha F}{RT}(E - E^{0'})\right] \quad (6)$$

where j_0 is the exchange current density, α is the symmetry transfer coefficient, $E^{0'}$ is the formal potential, and c_O^0 is the concentration value of species O in the bulk. If the charge transfer at the electrode is mass transport limited, the current can be calculated using Fick's first law.[39]

All the simulations were performed using COMSOL Multiphysics 3.3a (Comsol AB, Sweden) and Matlab 7.0.4 (MathWorks). The two-dimensional microband electrode model consisted of a plane perpendicular to the electrode surface, as it is shown in Figure 2. The values for the diffusion coefficients of ferrocyanide and ferricyanide, D, were both set to 6.5×10^{-10} m^2 s^{-1} [39] while the symmetry transfer coefficient, α, and the temperature were set to 0.5 and 298 K, respectively. The viscosity, η, of the flowing solution was taken as 10^{-3} Pa s while the density, ρ, was set to 10^3 kg m^{-3} (i.e., the viscosity and density of water at 25 °C).

RESULTS AND DISCUSSION

Electrode Characterization and Comparison with Simulations. Since the flow in the present microchannel was laminar, the diffusion layer thickness should be stable and reproducible and steady state voltammograms should be observed. This was also confirmed by the experiment as seen in Figure 3, which shows typical cyclic voltammetric responses of a gold microband electrode obtained with an equimolecular solution containing 5.0 mM ferrocyanide and ferricyanide in 0.5 M KNO_3 at different scan rates and a nominal flow rate of 5 μL min^{-1}. All the voltammograms present the expected sigmoidal shape, and it is also seen that the limiting current did not depend on scan rate. In these experiments, one of the gold bands was used as a quasi-reference electrode, and the potential of the latter was found to be −0.147 V vs SCE. The potential of the quasi-reference electrode was found to be stable during the experiments. The stability of the microband used as the working electrode was confirmed by comparing cyclic voltammograms at the same flow rate recorded prior to and after the experiments.

As the results in Figure 3 were obtained using a rather low flow rate (i.e., 5 μL min^{-1}), for which deviations from the Levich behavior could be expected, simulations were performed to investigate the influence of the flow rate on the steady state currents at low flow rates. Figure 4 shows the ratio between the current predicted by our two-dimensional model and the Levich equation (i.e., eq 2) for flow rates between 0 and 5 μL min^{-1}. The channel and electrode dimensions used in these simulations corresponded to those of the experimental device described in Figure 1. Figure 4 shows that the currents predicted by our model and the Levich equation are practically identical at high flow rates but that they become significantly different if the flow rate is decreased sufficiently. This can be explained by the fact that the Levich equation does not take neither edge diffusion at the microband electrodes nor channel wall effects into account. Thus, the limiting current may be underestimated by more than 5% for flow rates lower than 0.3 μL min^{-1} unless edge diffusion is considered. Our results show that radial diffusion at the edge of the microelectrodes needs to be taken into account at flow rates

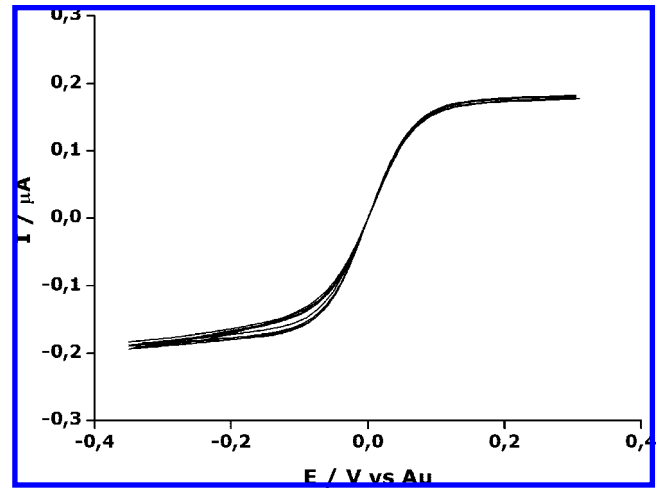

Figure 3. Cyclic voltammograms recorded at a scan rate of 25, 50, 75, and 100 mV s^{-1}, respectively, in a solution of 5.0 mM ferrocyanide, 5.0 mM ferricyanide, and 0.5 M KNO_3 at a flow rate of 5 μL min^{-1} with a gold microband as a quasi-reference electrode. The microbands were 20 μm wide, and the interelectrode distance was 50 μm.

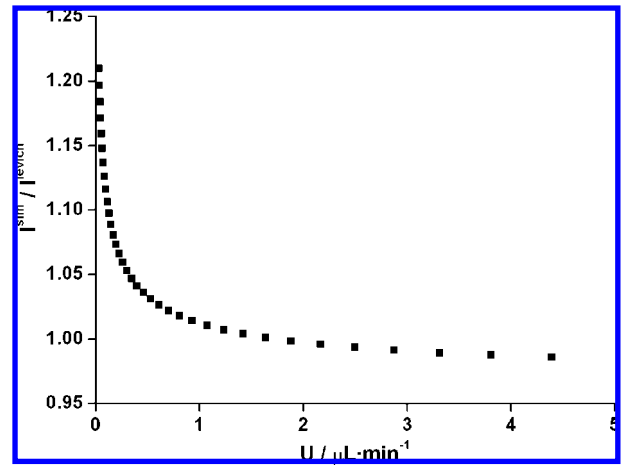

Figure 4. Limiting current ratio between the simulated currents, I^{sim}, and the Levich equation, I^{Levich}, as a function of the volumetric flow rate for a microband electrode (x_e = 20 μm, d = 95 μm) in a microchannel (d = 95 μm, $2h$ = 77 μm) containing a solution of 5.0 mM ferrocyanide, 5.0 mM ferricyanide, and 0.5 M KNO_3. The flow rate ranged from 0 to 5 μL min^{-1}.

for which the distortion of the diffusion layer due to the convection is lower. The latter effect is illustrated in parts A and B of Figure 5, which depict the diffusion layers for flow rates of 1 and 10 μL min^{-1}, respectively. As the flow rate is increased, the diffusion layer thickness is decreased so that the radial contribution at the "edge" of the electrode becomes negligible. The results of the simulations indicate that this is the case for flow rates higher than about 1 μL min^{-1}, which means that the influence of edge effects should be small for the flow rates (i.e., 1−10 μL min^{-1}) employed in this work.

Figure 6A shows plots of the simulated (△) and experimentally (■) obtained limiting currents, for a scan rate of 100 mV s^{-1}, as a function of the flow rate. The experimental currents were smaller than the simulated ones for all flow rates. As the syringe pump was indeed found to deliver the correct flow rate, we attribute

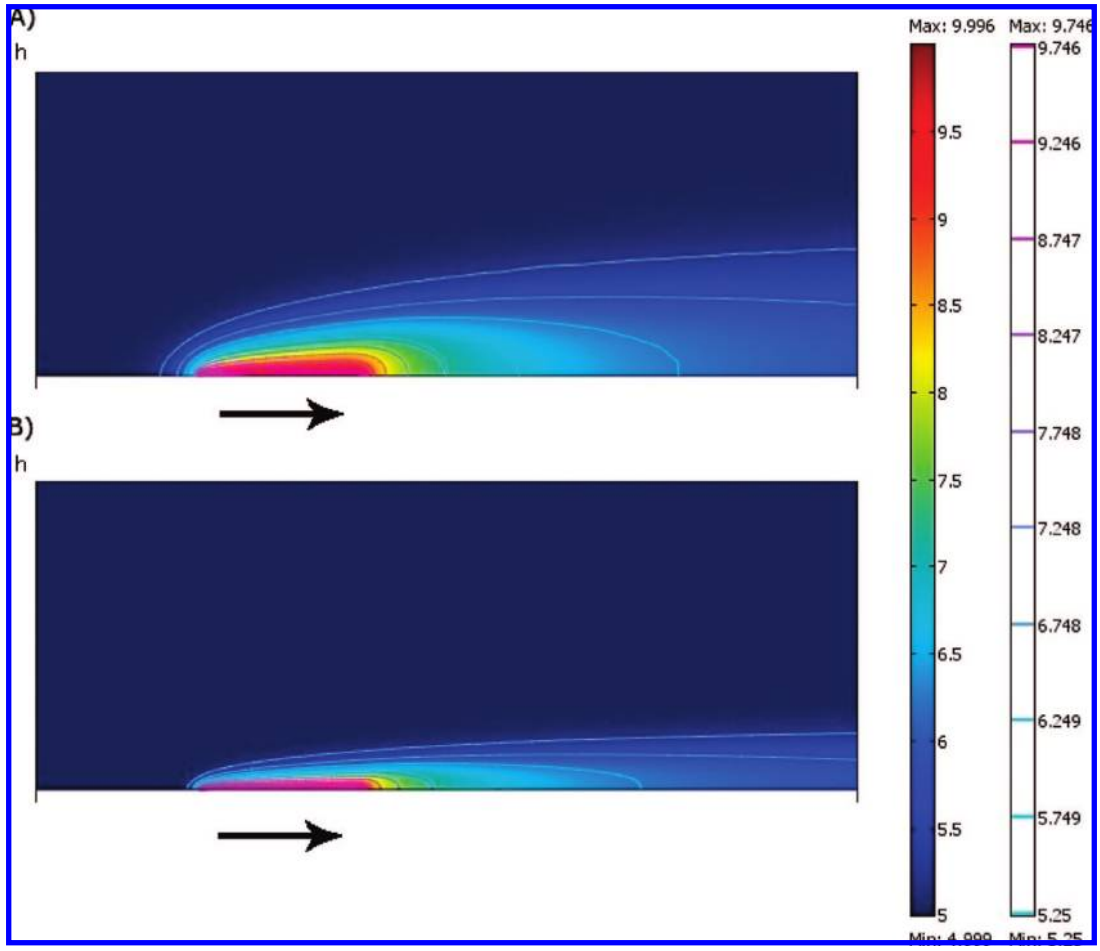

Figure 5. Simulated diffusion layers for a flow rate of (A) 1 and (B) 10 μL min^{-1}, respectively. The flow rates used corresponded to the minimum and the maximum flow rates used in the experiment. The arrows show the flow direction.

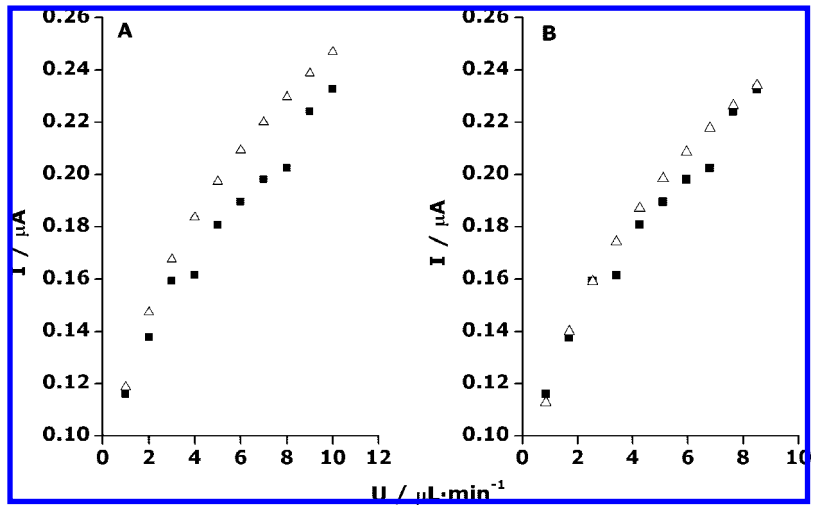

Figure 6. The experimental limiting voltammetric currents (■) and the corresponding simulated currents obtained with the two-dimensional model (△) as a function of the volumetric flow rate (A) before and (B) after correction for the presence of leaks. The uncorrected flow rates in part A ranged from 1 to 10 μL min^{-1} while the estimated real flow rate in part B ranged from 0.85 to 8.5 μL min^{-1}. The solution contained 5.0 mM ferrocyanide, 5.0 mM ferricyanide, and 0.5 M KNO_3, and the experimental results were obtained using a three-electrode configuration and a scan rate of 100 mV s^{-1}. The microbands were 20 μm wide, and the interelectrode distance was 50 μm.

these deviations in the current to the presence of tiny leaks at the inlet and outlet of the flow cell, which resulted in slightly lower flow rates. Such leaks are generally very difficult to eliminate completely in the present type of PDMS based microfluidic system. As a result, it is often difficult to predict (and determine) the real flow rate in the flow cells. However, by varying the flow

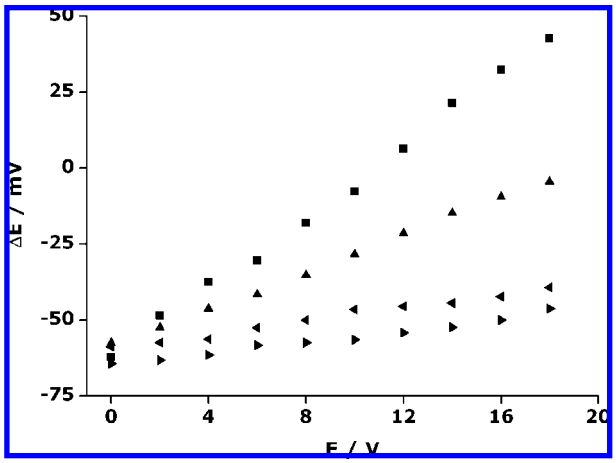

Figure 7. The potential difference between two gold microbands separated by 50 ("solid right triangle"), 120 ("solid left triangle"), 260 (▲), and 400 μm (■) in a solution of 0.5 M KNO_3 as a function of the external voltage difference. The corrected flow rate was 4.25 μL min^{-1}.

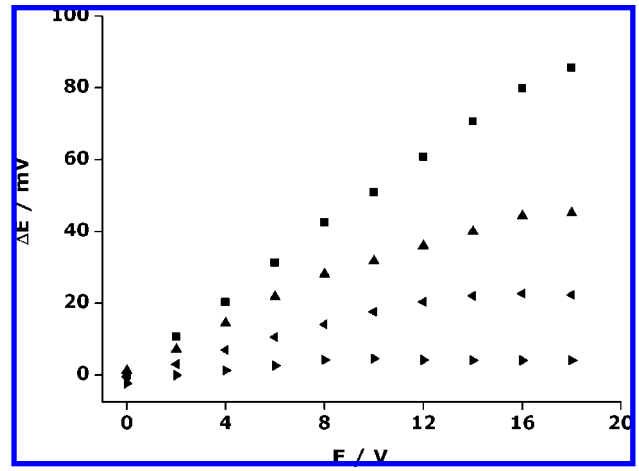

Figure 8. The potential difference between two gold microbands separated by 50 ("solid right triangle"), 120 ("solid left triangle"), 260 (▲), and 400 μm (■) in a solution of 5.0 mM $Fe(CN)_6^{4-}$, 5.0 mM $Fe(CN)_6^{3-}$, and 0.5 M KNO_3 for a corrected flow rate of 4.25 μL min^{-1} as a function of the external voltage difference.

rate used in the simulations and comparing the results of the simulations with the experimental currents, it is possible to estimate the real flow rate in the microfluidic cell. We have consequently used this approach to estimate the real flow rate in our microfluidic cell. As is seen in Figure 6B, the best fit between the experimental (■) and simulated (△) data was found for a flow rate that was about 85% of the nominal flow rate and all flow rates given below have hence been corrected using this correction factor.

Electric Field Induced Microband Potential Differences. As has been described by Klett and Nyholm,[33] the potential difference between two microbands induced by an external electric field can be used for potentiostatless amperometric end-column detection. In the present work, the same approach was used to study electric field induced electrochemical detection using an array of gold microband electrodes positioned within a PDMS microfluidic channel. Figure 7 shows the influence of the external voltage difference (E) on the potential difference (ΔE) between two bands positioned within the channel for different pairs of bands in 0.5 M KNO_3 and a flow rate of 4.25 μL min^{-1}. The distance between bands was 50 ("solid right triangle"), 120 ("solid left triangle";), 260 (▲), and 400 μm (■). As is seen in Figure 7, the dependence of ΔE on the applied external voltage difference was practically linear in all four cases. It is also evident that the magnitude of the potential difference between the electrodes increased with the interelectrode distance. The latter is in good agreement with the expectations based on the end-column results previously obtained by Klett and Nyholm.[33] The reproducibility of the results was checked by repeating the experiments at least four times. It was found that the differences between the slopes of the ΔE vs E plots were less than 8% in all cases. The linear dependence of the potential difference between the electrodes on the external voltage difference indicates that the potential difference was controlled merely by the ratio between the solution resistance between the electrodes (which increases with increasing interelectrode distance) and that of the microfluidic system as a whole. This finding also implies that the resistance between the electrodes was independent of the applied voltage difference. The latter is not unexpected since no species, able to undergo electrochemical reactions at the electrodes for these potential differences between the electrodes, should have been present in this solution.

As is seen in Figure 8, which shows the results obtained with a solution containing 5.0 mM ferrocyanide and 5.0 mM ferricyanide in 0.5 M KNO_3, the relationship between the difference in the potential between the microbands and the external voltage difference changed significantly when a redox couple was introduced into the flowing solution. It is seen that for all curves, except that for the largest difference in the distance between the microbands, the potential difference between the microbands reached a practically constant level for sufficiently large external voltage differences, although a linear dependence was seen for smaller external voltage differences. The attainment of the approximately constant potential differences can hence be ascribed to the presence of the ferro/ferricyanide couple which, acting as a depolarizer, modify the potential difference observed between microbands. This finding is in good agreement with previous results obtained by Klett and Nyholm.[33] In the presence of the ferro/ferricyanide redox couple, which can be considered a reversible redox couple, only a small potential difference between the electrodes would be needed to enable oxidation of ferrocyanide at one electrode and reduction of ferricyanide at the other electrode. In the presence of redox reactions, the oxidation current must clearly equal the reduction current and the rate of one of the redox reactions should therefore become rate limiting. The constant potential difference between the electrodes can then be seen as a mixed potential according to the mixed potential theory frequently employed in the discussion of corrosion experiments.[42] On the basis of this theory, the potential plateaus seen in Figure 8 can be explained by the fact that a small potential difference would be sufficient to support a (very small) current through the voltmeter in the presence of a reversible redox couple. It is also evident that the current could not have been mass transfer

(42) Jones, D. A. *Principles and Prevention of Corrosion*, 2nd ed.; Prentice Hall: Englewood Cliffs, NJ, 1996, p 86.

controlled since it should have been too small to induce any significant change in the surface concentrations of $Fe(CN)_6^{4-}$ and $Fe(CN)_6^{3-}$ due to the fact that a voltmeter with a high internal resistance was used in the experiments.

In analogy with Figure 7, the potential difference between the microbands increase with increasing interelectrode distance in Figure 8 as a result of the larger solution resistance between the electrodes. The fact that the value of the mixed potential plateau increased with increasing interelectrode distance can analogously be ascribed to the increased *iR* drop between the electrodes. The lack of an evident plateau for the largest distance between the electrodes in Figure 8 in fact suggests that the potential difference between these electrodes was controlled by the resistance between the bands (i.e., as in Figure 7) rather than by the solution equilibrium potential (mixed potential) in this case. In the absence of an added redox couple (see Figure 7), a much larger ΔE value would clearly be needed to induce electrochemical reactions (e.g., the oxidation and reduction of water) at the electrodes. This is in good agreement with the linear ΔE vs E relationship in Figure 7 for the same external voltage differences as used in Figure 8.

The results in Figures 7 and 8 clearly demonstrate that the potential difference between the two electrodes increases linearly with the external voltage as long as electrochemical reactions are unable to take place at the electrodes (i.e., as long as the induced potential difference between the electrodes is sufficiently small). In the presence of electroactive species in the solution, the external voltage induced potential differences between the electrodes depend both on the external electric field (ohmic polarization) and the chemical composition of the solution since the electrode potential will be a mixed potential in the presence of redox reactions at the electrodes. As the results in Figures 7 and 8 are in good agreement with the data previously obtained by Klett and Nyholm[33] in end-column experiments, it is clear that it should be possible to use the potential differences induced by an external voltage difference to induce electrochemical reactions on pairs of microband electrodes positioned anywhere within a microfluidic channel. In the presence of an external electric field, the current induced between an appropriately selected pair of microband electrodes could therefore be used for electrochemical detection of electroactive species in the flowing solution, as will be shown in the next section.

Electric Field Induced Microband Currents. In Figure 9, the induced current between pairs of microband electrodes separated by 250, 520, 790, and 1060 μm is shown as a function of the external voltage difference. These experiments, which were performed in a 0.5 M KNO_3 solution, clearly show that an increasingly larger external voltage difference was needed to induce a current as the distance between the microband electrodes was decreased. This can be explained by the fact that the potential difference, and thus the driving force, for the redox reactions at the microband electrodes depends on the interelectrode distance as depicted in Figure 7. For the smallest interelectrode distance of 250 μm, the largest external voltage difference was hence needed to obtain the potential difference required for the onset of redox reactions at the microband electrodes. For a sufficiently low external voltage difference, the induced potential difference between the microbands was hence not large enough to drive the oxidation

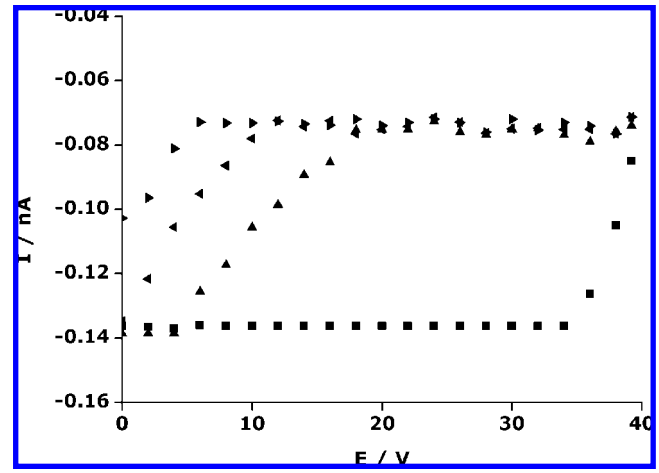

Figure 9. The induced current between two 20 μm wide microbands separated by 250 (■), 520 (▲), 790 ("solid left triangle"), and 1060 μm ("solid right triangle") as a function of the external voltage difference for a solution of 0.5 M KNO_3 at a corrected flow rate of 4.25 μL min^{-1}.

and the reduction reactions and the current was therefore equal to the baseline current given by the picoamperemeter offset current. The current observed for a zero nominal external voltage difference with an interelectrode distance of 1060 μm suggests that a small voltage difference was still present between the electrodes in this case. More importantly, Figure 9 shows that the same limiting current of about 0.06 nA was reached independently of the distance between the microband electrodes. The plots of the current as a function of the external voltage difference for the intermediate interelectrode distances are incidentally very similar to the steady state voltammograms seen in Figure 3. Similar results have likewise been obtained by Klett and Nyholm[33] in the end-column detection mode.

The fact that the same limiting current was found at least for the three largest interelectrode differences in Figure 9 indicates that the current was limited by mass transport of the same redox species in all these cases. Mass transport limitation is further supported by the fact that the total current through the microfluidic cell was found to be 21 μA for an external voltage difference of 40 V. The latter clearly shows that only a very small fraction (i.e., 3×10^{-4}%) of the total current flowed via the electrodes. In the 0.5 M KNO_3 solution, the likely redox reactions include reduction of dissolved oxygen and oxidation of gold, the Ti adhesion layer or impurities in the solution. The oxidation of the adhesion layer was possible since the microfabrication process employed resulted in electrodes for which the Ti adhesion layer was in contact with the electrolyte at the edges of the electrode (see below). Given an electrode area of 1.9×10^{-5} cm^2, the limiting current in Figure 9 corresponds to a current density of about 3 $\mu A/cm^2$. As this current density is approximately 1 order of magnitude smaller than the current density expected for mass transport controlled reduction of oxygen in a saturated quiescent solution, the current was most likely limited by the oxidation reaction. This hypothesis was verified by carrying out experiments in the presence of ascorbic acid, as shown in Figure 10. As the oxidation of ascorbic acid is irreversible, the presence of this compound should not affect the reduction process at the microband electrode acting as the

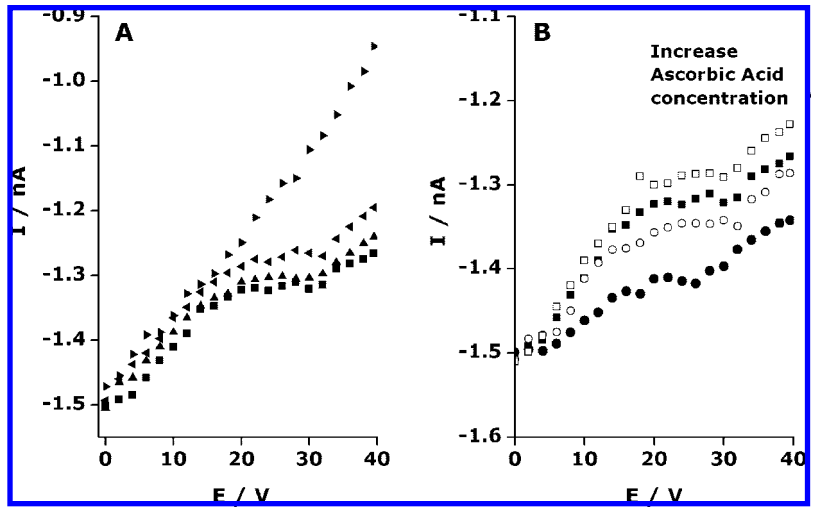

Figure 10. (A) The induced current between two 20 μm wide microbands separated by 50 (■), 120 (▲), 260 ("solid left triangle"), and 400 μm ("solid right triangle") as a function of the external voltage difference for a solution containing 0.5 M KNO_3 and 150 μM ascorbic acid. (B) The induced current between two 20 μm wide microbands separated by 50 μm as a function of the external voltage difference for increasing ascorbic acid concentrations from 50 to 200 μM in 0.5 M KNO_3. The corrected flow rate was 4.25 μL min^{-1}in both plots.

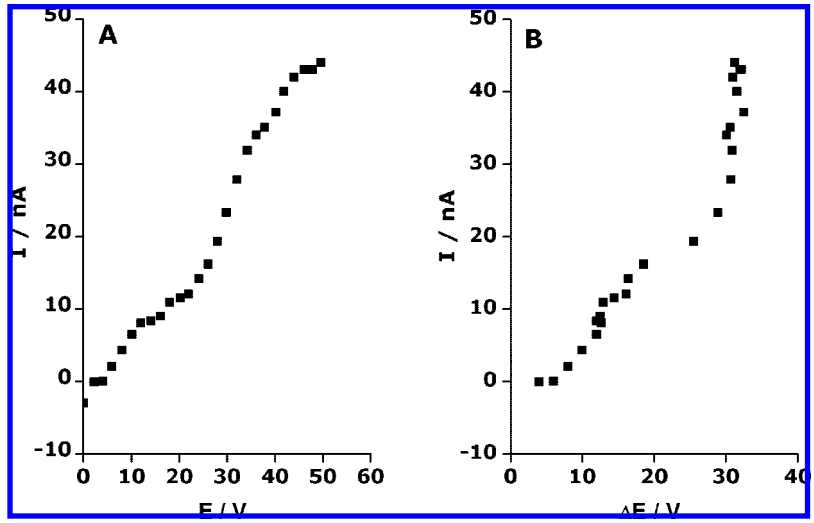

Figure 11. The induced current between two 20 μm wide microbands separated by 50 μm as a function of (A) the external voltage difference and (B) the potential difference between the microbands, respectively, for a solution containing 5.0 mM ferrocyanide, 5.0 mM ferricyanide, and 0.5 M KNO_3. The corrected flow rate was 4.25 μL min^{-1}.

cathode. Figure 10A shows that while very similar limiting currents were found for interelectrode distances of 50, 120, and 260 μm, a linear current versus external voltage difference plot was obtained for an interelectrode distance of 400 μm due to the significant influence of the *iR* drop in the latter case. The results for the three smallest distances indicate that well-defined steady state voltammograms with a significantly higher limiting current than in Figure 9 (i.e., about 10 $\mu A/cm^2$ compared to 3 $\mu A/cm^2$) were obtained when 150 μM ascorbic acid was added to the 0.5 M KNO_3 solution. This demonstrates that the current between the microband electrodes was controlled by the concentration of electroactive species in the solution. The exact concentration of ascorbic acid in the flowing solution was, however, difficult to calculate since a significant fraction of the ascorbic acid most likely was oxidized by the oxygen present in the solution. As presented in Figure 10B, experiments were therefore made with increasing ascorbic acid concentrations from 50 to 200 μM by successively adding ascorbic acid to the solution for an interelectrode distance of 50 μm. It is clearly seen that the limiting current increased as a result of these additions, which further supports the conclusion that the current was limited by the oxidation at the microband serving as the anode.

In Figure 11, it is seen that even larger limiting currents could be obtained when a solution containing a mixture of 5.0 mM $Fe(CN)_6^{4-}$ and 5.0 mM $Fe(CN)_6^{3-}$was used with the same interelectrode distance (i.e., 50 μm) as in Figure 10. In parts A and B of Figure 11, the current is plotted as a function of the external voltage difference and the measured potential difference between the electrodes, respectively. In Figure 11A, it is seen that a limiting current of about 10 nA, corresponding to a current density of about 0.5 mA/cm^2, was obtained for an external voltage difference of about 15 V. As is seen in Figure

11B, this external voltage difference corresponded to a potential of about 15 mV between the electrodes. The attainment of this current density for such a small potential difference is in good agreement with the fact that a reversible redox couple was present in the solution. An addition of 5.0 mM $Fe(CN)_6^{4-}$ and $Fe(CN)_6^{3-}$ to the solution thus resulted in an increase in the current density by almost 2 orders of magnitude compared to that obtained in 0.5 M KNO_3 in Figure 9. This clearly shows that the current between the electrodes is limited by the redox reactions at the electrodes and that the induced current between two microband electrodes can be used for analytical purposes. After the experiments in the $Fe(CN)_6^{3-}/Fe(CN)_6^{4-}$ solution described above, it was, however, found that the area of the electrode that had served as the anode had decreased significantly due to a partial detachment of the gold layer. As a result of this loss of the gold layer, the electrodes were severely damaged already after a few experiments. We attribute this effect to an oxidation of the Ti adhesion layer resulting in a partial loss of the gold layer as described by Nilsson et al.,[43] who found that oxidation of titanium adhesion layers can take place via pinholes and cracks in the gold layer. The corresponding reaction should in the present case have been facilitated by the fact that the edges of the adhesion layer were in direct contact with the electrolyte. In Figure 11B, it is therefore possible that this reaction was involved in the rapid increase in the current for potential differences between the electrodes larger than about 25 mV in Figure 11B. These results clearly show that the stability of the microband electrodes is an important issue and that care must be taken to ensure that the adhesion layer is not in contact with the electrolyte during the measurements. On the basis of the present results, it is thus very difficult to provide a relevant estimation of the reproducibility and long-time stability of the electrode responses for any of the analytes used in the present work. As will be shown elsewhere,[44] the electrode stability problem can, however, be circumvented by modifying the microfabrication procedure used in the manufacturing of the microband electrode. It should also be mentioned that the need for electrode long-time stability should be less with the approach described in the present work since a new pair of detection electrodes with the same interelectrode distance in the array could be used.

In the electric field induced current experiments, problems due to the presence of gas bubbles were also sometimes encountered. In these cases, the experiments were stopped and the cell was flushed with water or ethanol to remove the bubbles. According to our experience, the bubbles generally stem from oxygen or hydrogen formed as a result of a too large potential difference between the detection electrodes. One way to minimize this problem is thus either to reduce the distance between the electrodes or to employ lower electric field strengths. In a CE separation, the latter would be less attractive as it would affect the separation time and quality significantly. A better solution hence involves the use of electrode arrays with many electrodes and small interelectrode distances, with which it always would be possible to find two electrodes with an interelectrode potential large enough to enable the detection but small enough to ensure no formation of oxygen or hydrogen. Oxygen (or hydrogen) bubbles can, naturally, also be formed at the "high-voltage" electrodes used to induce the electric field in the flow channel. As the influence of the latter problem depends on the magnitude of the (CE) current and the current density at the "high-voltage" electrodes, the resistance of the channel (or capillary) and the area of the "high-voltage" electrodes should generally be made as large as possible. More importantly, the present results clearly show that it is possible to carry out electric field driven electrochemical detection anywhere within a microfluidic channel without interferences from the applied electric field.

CONCLUSIONS

It has been shown that electrochemical detection can be carried out within a microfabricated channel containing an appropriately positioned array of gold microband electrodes in the presence of an external electric field. The detection, which is driven by the potential difference induced between two microband electrodes, is consequently not dependent on the use of a decoupler such as those commonly employed in electrochemical detection in capillary electrophoresis at the present time.

The present results, which also include simulations of the flow rate dependence of the current at microliter per minute flow rates, clearly show that potential difference between the two microband electrodes depends on the external electric field strength and the distance between the electrodes in the electric field. This means that the potential difference between two microband electrodes can be adjusted to enable the detection of different electroactive species merely by selecting the appropriate electrode pair in an array of microband electrodes. The resulting current between the microband electrodes has been shown to depend on the concentration of the electroactive species in the solution and by plotting the current as a function of the external voltage difference, steady state voltammograms, analogous to those obtained in conventional potentiostatic measurements, can in fact be obtained. Oxidative detection is facilitated by the fact that the solution contains dissolved oxygen which can support the required reduction at the microband serving as the cathode.

To ensure long-term detection stability, care must be taken to eliminate oxidation of the adhesion layers of the microband electrodes by making sure that there is no contact between the adhesion layers and the electrolyte. This can be obtained by making sure that the edges of the adhesion layer are covered by an appropriate insulating layer during the microfabrication step.

The results of the 2D simulations demonstrate that edge diffusion effects can be neglected for flow rates higher than about 1 μL min^{-1} (i.e., linear flow rates larger than 0.23 cm s^{-1}) and that comparisons between the experimental and simulated results can be used to detect the presence of tiny leaks that otherwise may be difficult to spot.

As standard microfabrication procedures can be used to produce microband array electrodes with excellent control of the electrode dimensions, positions, and interelectrode distances, the present electrochemical detection approach is well-suited for use

(43) Nilsson, S.; Klett, O.; Svedberg, M.; Amirkhani, A.; Nyholm, L. *Rapid Commun. Mass Spectrom.* **2003**, *17*, 1535–1540.
(44) Karlsson, M.; Ordeig, O.; Nikolajeff, F.; Nyholm, L. In preparation.

in electrochemical chip based systems. Although this development clearly is facilitated by the ease by which flow channels of PDMS can be manufactured, it would also be possible to employ microfluidic channels of other materials. We therefore believe that the present electric field driven electrochemical detection technique can contribute to the development of new inexpensive and portable devices for the analysis of species based on, for example, capillary electrophoresis.

ACKNOWLEDGMENT

Financial support from the Swedish Research Council (Grant 621-2005-5493) is gratefully acknowledged. N. Godino and O. Ordeig would like to thank the Spanish Ministry of Science and Education for financial support through the I3P Program. F. Javier del Campo gratefully acknowledges funding through Ramón y Cajal fellowship. Also, O.O. would like to thank Dr. Sara Thorslund and Dr. Mikael Karlsson for their very fruitful help during the device fabrication.

Received for review December 19, 2007. Accepted February 27, 2008.

AC702570P